Journal of Process Control 21 (2011) 1504–1516

Contents lists available at ScienceDirect

Journal of Process Control

journal homepage: www.elsevier.com/locate/jprocont

A distributed control framework for smart grid development: Energy/water system optimal operation and electric grid integration

Wei Qi[a], Jinfeng Liu[a], Panagiotis D. Christofides[a,b,*]

[a] Department of Chemical and Biomolecular Engineering, University of California, Los Angeles, CA 90095-1592, USA
[b] Department of Electrical Engineering, University of California, Los Angeles, CA 90095-1592, USA

ARTICLE INFO

Article history:
Received 14 December 2010
Received in revised form 26 May 2011
Accepted 26 May 2011
Available online 1 July 2011

Keywords:
Electrical grid
Renewables-based energy generation systems
Water systems
Supervisory predictive control

ABSTRACT

In this work, we propose a conceptual distributed control framework for electrical grid integrated with distributed renewable energy generation systems in order to enable the development of the so-called "smart electrical grid". First, we introduce the key elements and their interactions in the proposed control architecture and discuss the design of the distributed control systems which are able to coordinate their actions to account for optimization considerations on the system operation. Subsequently, we focus on a specific wind/solar energy generation system connected to a reverse osmosis water desalination system and the electrical grid and design two supervisory predictive controllers via model predictive control to operate the integrated system taking into account short-term and long-term optimal maintenance and operation considerations, respectively. Simulations are carried out to illustrate the applicability and effectiveness of the proposed approach.

1. Introduction

The traditional electrical grid involves large, centralized power plants that feed power over an electro-mechanical grid to end users using one-directional power flows. While the traditional electrical grid has been successful, in recent years there have been numerous calls for the development of "smart" electrical grid (e.g., Refs. [1–4]) by expanding the traditional electrical grid with distributed, medium-scale renewables-based energy generation systems and digital technologies, for example, communications, computing, sensing and automation, to better meet the increasing energy demand and environmental regulations. Incorporated with two-way communication networks, digital devices and distributed optimization and control systems, the so-called "smart grid" is expected to be more reliable, more secure, more energy efficient and more environmentally friendly. One important feature of the smart grid is its capability of integrating distributed energy resources and generation, for example, renewable energy resources, into the electrical grid. Renewable energy resources, like wind and solar-based energy generation systems, are receiving national and worldwide attention owing to the rising rate of consumption of fossil fuels. In addition to the environmental benefits, solar and wind renewable energy generation systems also have a reduced investment risk and an increased energy efficiency. However, integrating renewable energy generation systems with the electrical grid requires addressing key fundamental challenges, for example, variable output, in the operation of intermittent renewable resources like solar- and wind-based energy generation systems. One approach to deal with the variable output of wind and solar energy generation systems is through the use of energy generation systems using both wind and solar energy integrated with loads, the electrical grid and distributed energy storage systems.

In the literature, most of the results on the control of wind and solar systems have focused on wind or solar systems. Specifically, there is a significant body of literature dealing with control of wind-based energy generation systems (see, for example, Refs. [5–16] for results and references in this area), while several contributions have been made to the control of solar-based energy generation systems (see, for example, Refs. [17–21]). There are also a few pieces of work on the regulation of stand-alone [22–25] and grid-connected [26,27] hybrid wind-solar energy generation systems. However, no attention has been given to the development of supervisory control systems for hybrid wind-solar energy generation systems that take into account system maintenance and optimal system operation considerations, except for our recent efforts [28,29]. Specifically, in Ref. [28], we proposed a supervisory predictive control method for short-term optimal management and operation of wind-solar energy generation systems in which the supervisory control system was designed via model predictive control (MPC) to take into account optimal allocation of generation assignment between the two subsystems. In Ref. [29], we

* Corresponding author at: Department of Chemical and Biomolecular Engineering, University of California, Los Angeles, CA 90095-1592, USA.
E-mail address: pdc@seas.ucla.edu (P.D. Christofides).

0959-1524/$ – see front matter © 2011 Elsevier Ltd. All rights reserved.
doi:10.1016/j.jprocont.2011.05.010

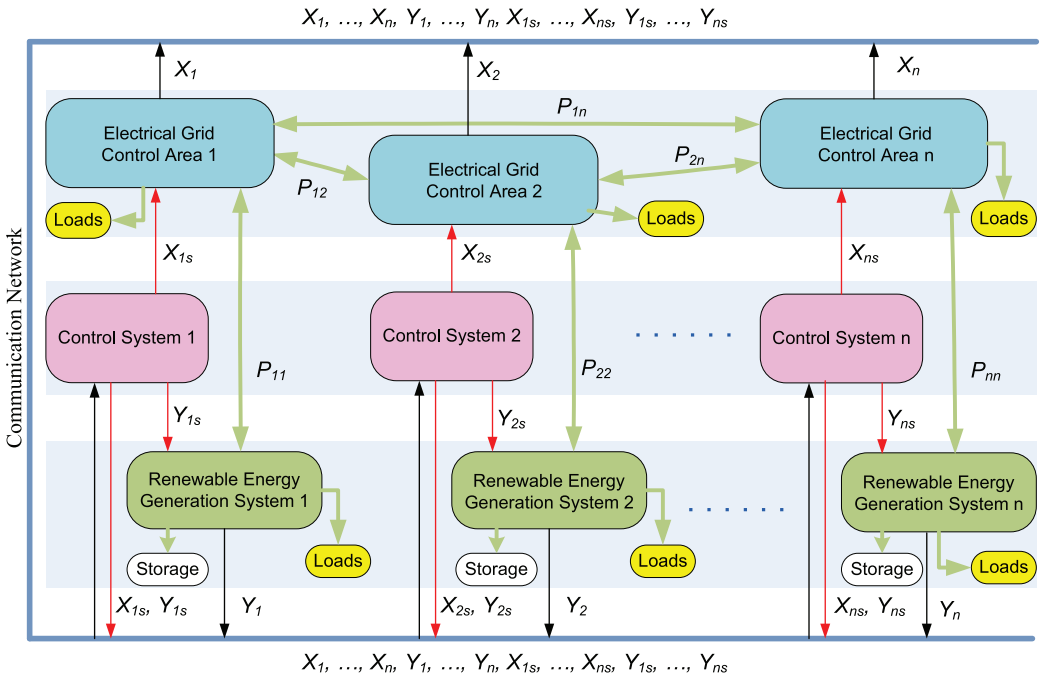

Fig. 1. Electrical grid integrated with renewable energy generation systems, storage, loads and distributed control systems.

designed a computationally efficient supervisory control system for long-term optimal management and operation of an integrated wind-solar energy generation and a reverse-osmosis (RO) water desalination system, based on a two-time-scale decomposition of the integrated system model.

In this work, we propose a conceptual distributed control framework for electrical grid integrated with distributed renewable energy generation systems in order to enable the development of the so-called "smart electrical grid". First, we introduce the key elements and their interactions in the proposed control architecture and discuss the design of the distributed control systems which are able to coordinate their actions to account for optimization considerations on the system operation. Subsequently, we focus on a specific wind/solar energy generation system connected to a reverse osmosis desalination system and the electrical grid and design two supervisory predictive controllers via model predictive control to operate the integrated system taking into account short-term and long-term optimal maintenance and operation considerations, respectively. In the long-term operation case, the wind/solar/water system is assumed to be integrated into the electrical grid and is able to trade power with the electrical grid with explicit consideration of real-time electricity pricing. Simulations are carried out to illustrate the applicability and effectiveness of the proposed supervisory predictive controllers.

2. Distributed control architecture for integrating distributed energy resources and loads to the electrical grid

The proposed distributed control architecture for electrical grid integrated with distributed renewable energy generation systems and distributed loads is shown in Fig. 1. The key elements of the proposed control architecture include an electrical grid divided into several control areas, distributed renewable energy generation systems, distributed control systems and a real-time communication network.

In the architecture shown in Fig. 1, we consider that the electrical grid is decomposed into n control areas. Each control area typically consists of numerous generators and loads. The different control areas are interconnected through bi-directional power lines and electrical power can flow between the different control areas bi-directionally via the power lines. For example, in Fig. 1, electrical power can flow from control area 1 to the other control areas (e.g., control areas 2 to n) and be transmitted to control area 1 from other control areas. The symbol P_{ij} $(i = 1, \ldots, n \quad \text{and} \quad j = 1, \ldots, n)$ is used to denote the power transmitted between control areas i and j. When the energy generated in a control area is not enough to satisfy the total power demands in that control area, the energy-deficient control area may obtain additional energy from other control areas or its associated renewable energy generation system. When the energy generation in a control area is sufficient and there is a surplus of energy, this area may transmit energy to other control areas or its associated loads or storage systems.

Each of the electrical grid control areas may connect with many different types of renewable energy generation systems. To simplify the description, in Fig. 1, we assume that all the renewable energy generation systems connected to a control area can be lumped into one equivalent renewable energy generation system which is also connected with the control area using bi-directional power lines. A renewable energy generation system first uses its generated energy to satisfy the loads connected to it and also sends, if the generation capacity permits, extra energy produced to its associated control area. If the energy generated by a renewable energy generation system is not sufficient to satisfy its load demands, it may also get energy from its associated control area. In Fig. 1, the symbol P_{ii} $(i = 1, \ldots, n)$ is used to denote the power transmitted between control area i and the renewable energy generation system i.

We propose to design a control system for each control area and its associated renewable energy generation system. The control system calculates the operating set-points for the control area and the renewable energy generation system. There is also a real-time communication network integrated in the overall system. The control areas, renewable energy generation systems and the control systems communicate via the real-time communication network at specific sampling time instants. In Fig. 1, the symbols X_i and Y_i $(i = 1, \ldots, n)$ are used to indicate the state of control area i and of the renewable energy generation system i; the symbols X_{is} and Y_{is} $(i = 1, \ldots, n)$ are used to indicate the operating set-points calcu-

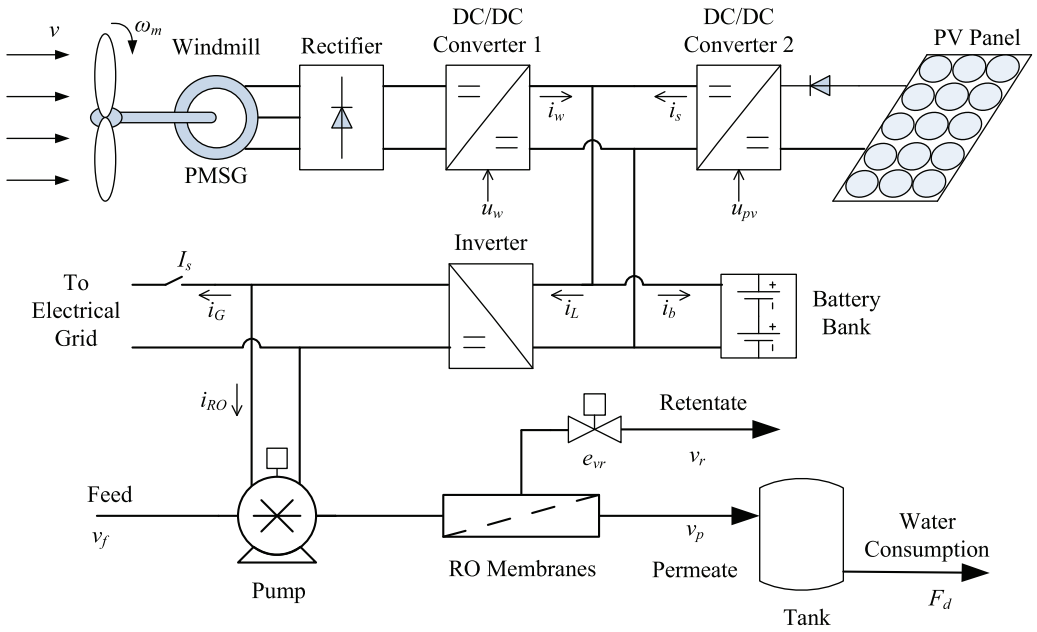

Fig. 2. Integrated wind/solar energy generation and water desalination system.

lated by control system i for the control area i and renewable energy generation system i. At a sampling time t_k, control areas and renewable energy generation systems broadcast their state information at t_k (i.e., $X_1(t_k), \ldots, X_n(t_k)$, $Y_1(t_k), \ldots, Y_n(t_k)$) to the communication network, and the control systems also broadcast their last control actions (e.g., control system i broadcasts $X_{is}(t_{k-1})$, $Y_{is}(t_{k-1})$) to the communication network and receive all the state and control actions information at t_k. Based on the state information and control actions of other control systems, control system i calculates its own control actions (i.e., $X_{is}(t_k)$ and $Y_{is}(t_k)$). In the design of the distributed control systems, model predictive control, especially distributed MPC, is particularly suited because of its ability to account for the control actions of other control systems and its ability to take into account optimization considerations and constraints in the calculation of control actions in real-time. There are some distributed MPC designs that have been proposed in the literature [30–33] (see also Ref. [34] for an application of distributed MPC to power system) which are very suitable for this control problem and currently being explored by our group.

The successful development of the proposed distributed control architecture needs to address many key challenging issues including: (1) the predictive control of different types of renewables-based energy generation systems, for example, integrated wind and solar energy generation systems, (2) the coordination of a renewables-based energy generation system with the electrical grid and loads, and (3) the cooperation between different control systems. In this work, we will focus on an integrated wind/solar energy generation system which is connected to an RO water desalination system and the electrical grid and design control systems to address the first two issues.

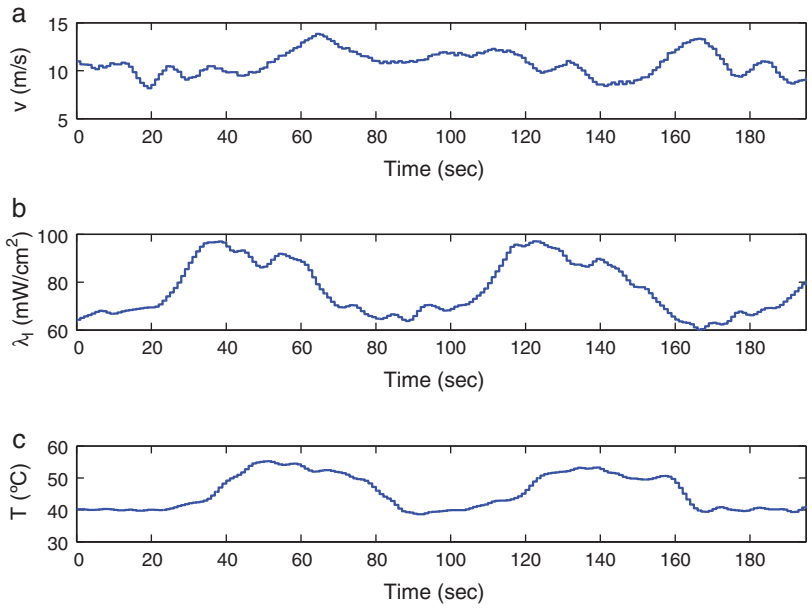

Fig. 3. Environmental conditions. (a) Wind speed v; (b) insolation λ_I; and (c) PV panel temperature T.

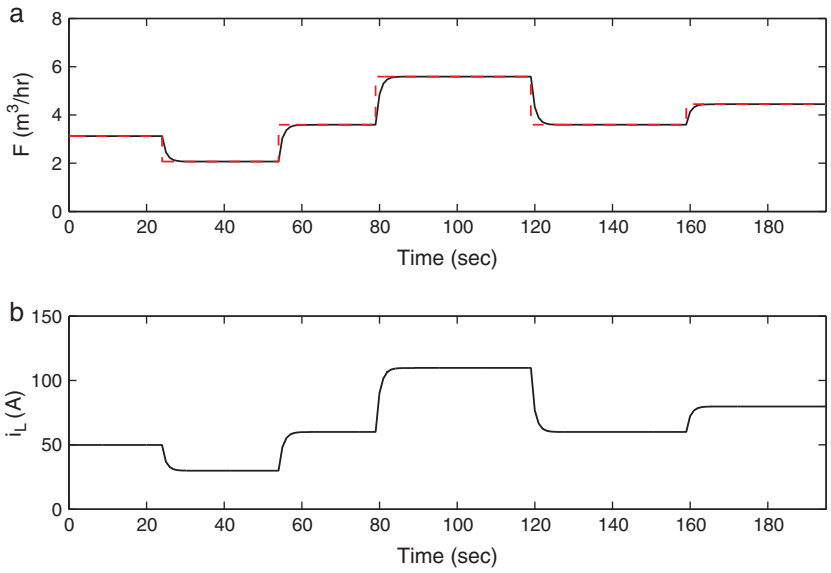

Fig. 4. (a) Time-varying water demand (dashed line) and actual water production (solid line) and (b) corresponding load current i_L.

3. Integrated wind/solar/RO system modeling

In this section, we introduce the integrated wind/solar energy generation system which is connected to an RO water desalination system and the electrical grid. A schematic of the integrated system is shown in Fig. 2.

3.1. Energy generation system description

There is a wind generation subsystem, a solar generation subsystem and a lead-acid battery bank which is used to overcome periods of scarce generation as well as store energy in the energy generation system.

Specifically, in the wind generation subsystem, there is a windmill, a multipolar permanent-magnet synchronous generator (PMSG), a rectifier, and a DC/DC converter. The DC/DC converter is used to control the operating point of the wind generation subsystem. The mathematic description of the wind subsystem written in a rotor reference frame is as follows [22]:

$$\begin{aligned}\dot{i}_q &= -\frac{r_s}{L}i_q - \omega_e i_d + \frac{\omega_e \phi_{sr}}{L} - \frac{\pi v_b i_q u_w}{3\sqrt{3}L\sqrt{i_q^2+i_q^2}}\\ \dot{i}_d &= -\frac{r_s}{L}i_d - \omega_e i_q - \frac{\pi v_b i_d u_w}{3\sqrt{3}L\sqrt{i_q^2+i_d^2}}\\ \dot{\omega}_e &= \frac{P}{2J}\left(T_t - \frac{3}{2}\frac{P}{2}\phi_{sr} i_q\right)\end{aligned} \tag{1}$$

where i_q and i_d are the quadrature current and the direct current in the rotor reference frame, respectively, r_s and L are the per phase resistance and inductance of the stator windings, respectively, ω_e is the electrical angular speed, ϕ_{sr} is the flux linked by the stator windings; v_b is the voltage on the battery bank terminals, u_w is the control signal (duty cycle of the DC/DC converter (DC/DC converter 1 in Fig. 2)), P is the PMSG number of poles, J is the inertial of the rotating parts and T_t is the wind turbine torque. The wind turbine torque can be written as:

$$T_t = \frac{1}{2}C_t(\lambda)\rho A R v^2 \tag{2}$$

where ρ is the air density, A is the turbine-swept area, R is the turbine radius, v is the wind speed, and $C_t(\lambda)$ is a nonlinear torque coefficient which depends on the tip speed ratio ($\lambda = R\omega_m/v$ with $\omega_m = 2\omega_e/P$ being the angular shaft speed).

Based on Eq. (1), we can express the power generated by the wind subsystem and injected into the DC bus as follows:

$$P_w = i_w v_b \tag{3}$$

where $i_w = (\pi/(2\sqrt{3}))\sqrt{i_q^2+i_d^2}u_w$ denotes the current which is injected to the DC bus by the wind subsystem.

In the solar generation subsystem, there is a photo-voltaic (PV) panel array and a half-bridge buck DC/DC converter (DC/DC converter 2 in Fig. 2). In this subsystem, similar to the wind subsystem, the converter is used to control the operating point of the PV panels. The mathematic description of the solar subsystem is as follows [23]:

$$\begin{aligned}\dot{v}_{PV} &= \frac{i_{PV}}{C} - \frac{i_s}{C}u_{PV}\\ \dot{i}_s &= -\frac{v_b}{L_c} + \frac{v_{PV}}{L_c}u_{PV}\\ i_{PV} &= n_p I_{ph} - n_p I_{rs}\left(\exp\left(\frac{q(v_{PV}+i_{PV}R_s)}{n_s A_c K T}\right) - 1\right)\end{aligned} \tag{4}$$

where v_{PV} is the voltage level on the PV panel array terminals, i_s is the current injected on the DC bus, C and L_c are electrical parameters of the buck converter, u_{PV} is the control signal (duty cycle), i_{PV} is the current generated by the PV array, R_s is the series resistance in the PV circuit, n_s is the number of PV cells connected in series, n_p is the number of series strings in parallel, K is the Boltzman constant, A_c is the cell deviation from the ideal p–n junction characteristic, I_{ph} is the photocurrent, and I_{rs} is the reverse saturation current. The power injected by the PV solar module into the DC bus can be computed by:

$$P_s = i_s v_b. \tag{5}$$

Note that this power indirectly depends on the control signal u_{PV}.

The lead-acid battery bank may be modeled as a voltage source E_b connected in series with a resistance R_b and a capacitance C_b. Based on this simple model, the DC bus voltage expression can be written as follows:

$$v_b = E_b + v_c + i_b R_b, \tag{6}$$

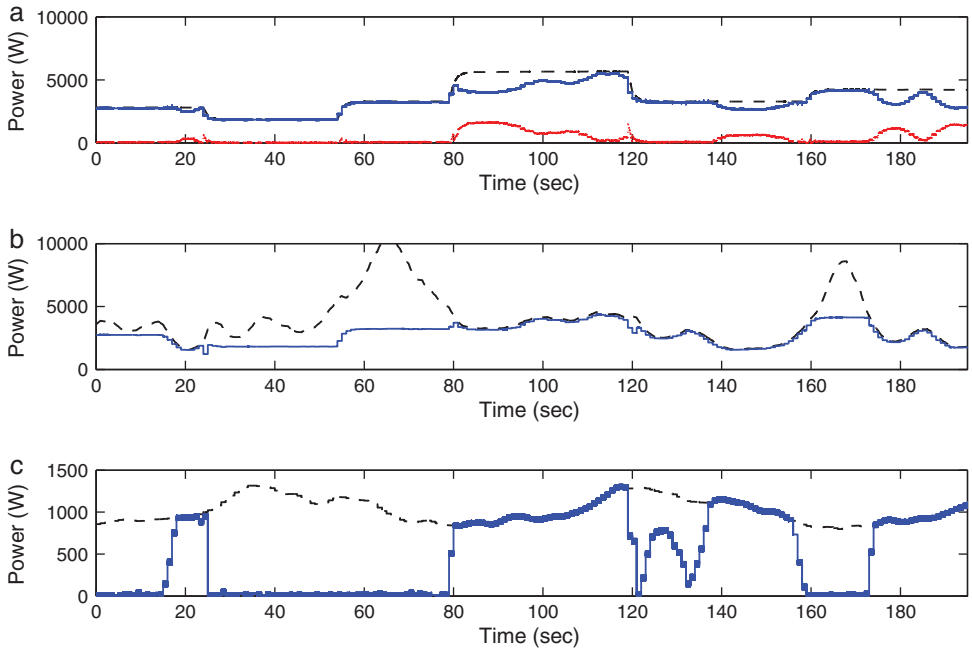

Fig. 5. (a) Generated power $P_w + P_s$ (solid line), total power demand P_T (dashed line) and power provided by battery bank P_b (dotted line); (b) Power generated by wind subsystem P_w (solid line) and maximum wind generation $P_{w,max}$ (dashed line); and (c) Power generated by solar subsystem P_s (solid line) and maximum solar generation $P_{s,max}$ (dashed line).

where i_b is the current across the battery bank, v_c is the voltage in capacitor C_b and its dynamics is as follows:

$$\dot{v}_c = \frac{1}{C_b} i_b. \tag{7}$$

The quantity of electricity stored in the battery bank can be calculated as follows:

$$Q_c = C_b v_c. \tag{8}$$

Based on Eq. (8), the state of charge (SOC) of the battery bank, s_b, can be calculated as follows:

$$s_b = \frac{Q_c}{Q_c^{max}} = \frac{v_c}{v_c^{max}} \tag{9}$$

where Q_c^{max} is the maximum capacity of the capacitor corresponding to the maximum voltage v_c^{max} that can be tolerated by the capacitor. We also introduce the concept of depth of discharge of the battery bank and denote it as d_b, which is calculated as follows:

$$d_b = 1 - s_b. \tag{10}$$

The integrated system has two operating modes. A binary variable, I_s, is used to indicate the operating mode of the integrated system. When $I_s = 1$, the integrated system is connected to the electrical grid; and when $I_s = 0$, the integrated system works in stand-alone mode. Assuming an ideal voltage inverter, we can write an energy balance equation as follows:

$$P_w + P_s = P_{RO} + I_s P_G + i_b v_b, \tag{11}$$

where P_{RO} denotes the total power demand from the water desalination system and the term $I_s P_G$ is used to denote the power sent to the electrical grid. Note that when i_b is positive, the battery bank is being charged and when i_b is negative, the battery bank supplies energy to the RO water desalination system or to the electrical grid. The energy balance of Eq. (11) can be also expressed in the form of current balance as follows:

$$i_w + i_s = i_{RO} + I_s i_G + i_b, \tag{12}$$

where i_{RO} and i_G are the currents injected to the RO water desalination system and the electrical grid, respectively. From Eq. (12), we obtain the current across the battery bank as follows:

$$i_b = i_w + i_s - i_{RO} - I_s i_G. \tag{13}$$

3.2. Water desalination system description

There is a high-pressure pump, a membrane module and a water storage tank in the RO water desalination system. Salt water is fed into the system through the pump, which is equipped with a variable frequency drive. The feed water is pressurized to a desired pressure [35] in the pump and then is sent to the membrane module where it is separated into a low-salinity product (or permeate) stream, and a high-salinity brine (or retentate) stream. The permeate stream enters the storage tank which provides desalinated water to satisfy the water consumption demand. Note that the difference between the water drawn from (water consumption) and the water fed into (water production) the storage tank is accumulated in the storage tank.

In the RO system, the pressure downstream of the actuated valve and at the permeate outlet is assumed to be equal to atmospheric pressure. The RO system model is based on a mass balance taken around the entire system and an energy balance taken around the actuated retentate valve as follows [35]:

$$\frac{dv_r}{dt} = \frac{P_{sys} A_p}{\rho_w V} - \frac{1}{2} \frac{A_p e_{vr} v_r^2}{V} \tag{14}$$

where v_r is the retentate stream velocity, P_{sys} is the feed pressure, A_p is the pipe cross-sectional area, V is the system volume, ρ_w is the fluid density, and e_{vr} is the retentate valve resistance. The system pressure P_{sys} can be calculated as follows:

$$P_{sys} = \frac{\rho_w A_p}{A_m K_m} (v_f - v_r) + \Delta\pi. \tag{15}$$

where A_m is the membrane area, K_m is the membrane overall mass transfer coefficient, v_f is the feed stream velocity, and $\Delta\pi$ is the dif-

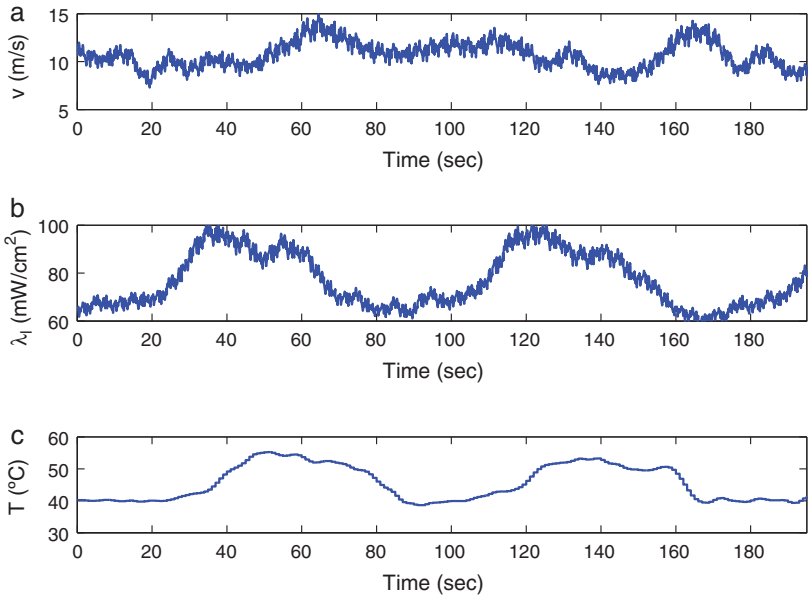

Fig. 6. Environmental conditions. (a) Wind speed v; (b) insolation λ_I; and (c) PV panel temperature T.

ference in osmotic pressure between the feed side of the membrane and the permeate side and can be computed by [35]:

$$\Delta\pi = \delta C_{\text{eff}}(T_{\text{w}} + 273)$$

where C_{eff} is the effective average concentration at the membrane surface, δ is a constant relating effective concentration to osmotic pressure and T_{w} is the water temperature in degrees Celsius.

Note that the three velocities v_{f}, v_{r} and v_{p} (the permeate stream velocity) satisfy an overall steady-state mass balance as follows (since all pipe cross-sectional areas are assumed to be the same):

$$0 = v_{\text{f}} - v_{\text{r}} - v_{\text{p}}. \tag{16}$$

Using the above dynamic equation, various control techniques can be applied using the valve resistance value (e_{vr}) as the manipulated input.

We operate the RO system at energy optimal water recovery, Y_{opt}, which requires that $v_{\text{p}}/v_{\text{f}}$ is adjusted in real time [36,37]. Based on the Bernoulli equation and ignoring the water elevation change, we can obtain the power needed for the water desalination system as follows:

$$P_{\text{RO}} = \frac{1}{\eta}\left(P_{\text{sys}}\frac{F_{\text{p}}}{Y_{\text{opt}}} + \frac{1}{2}\frac{F_{\text{p}}^3}{Y_{\text{opt}}^3 A_{\text{p}}^2}\rho_{\text{w}}\right), \quad 0 < \eta < 1 \tag{17}$$

where η is the overall power efficiency of the pump of the RO desalination system and $F_{\text{p}} = A_{\text{p}}v_{\text{p}}$ is the permeate flow rate (i.e., desalinated water production rate) which is used to satisfy the water consumption and storage demands. If we denote the water consumption demand as F_{d} and water storage demand as F_{s}, then we obtain the following equation from a steady-state mass balance:

$$0 = F_{\text{p}} - F_{\text{d}} - F_{\text{s}}. \tag{18}$$

Note that the water storage demand F_{s} can take positive or negative values.

Based on the Eqs. (16) and (18), the dynamics of the water level in the storage tank, h_{l}, can be obtained as follows:

$$\dot{h}_{\text{l}} = \frac{F_{\text{s}}}{A_{\text{s}}} = \frac{A_{\text{p}}}{A_{\text{s}}}(v_{\text{f}} - v_{\text{r}}) - \frac{F_{\text{d}}}{A_{\text{s}}} \tag{19}$$

where A_{s} is the cross-sectional area of the water storage tank. Similarly, we define the state of storage (SOS), s_{t}, for the storage tank as follows:

$$s_{\text{t}} = \frac{h_{\text{l}}}{h_{\text{l}}^{\max}}$$

where $h_{\text{l}}^{\max}$ is the maximum water level in the storage tank.

The dynamics of the integrated wind/solar/RO system can be written in the following compact form:

$$\begin{aligned} \dot{x} &= f(x) + g(x)u \\ h(x) &= 0 \end{aligned} \tag{20}$$

where $x = [i_{\text{q}}\ \ i_{\text{d}}\ \ \omega_{\text{e}}\ \ v_{\text{PV}}\ \ i_{\text{s}}\ \ v_{\text{c}}\ \ v_{\text{r}}\ \ h_{\text{l}}]^T$, $u = [u_{\text{w}}\ \ u_{\text{PV}}\ \ e_{\text{vr}}]^T$, and f, g, h are nonlinear vector functions whose explicit forms are omitted for brevity.

For the wind subsystem, the solar subsystem, the battery bank and the RO water desalination system, each of them has an associated local controller which is able to regulate them to track appropriate operating set-points. For the wind subsystem controller, the objective is to force the wind subsystem to track the operating trajectory, which is the desired power generation (power reference), $P_{\text{w}}^{\text{ref}}$. We follow the controller design proposed in Ref. [12] to design the local controller for the wind subsystem. For the solar subsystem controller, the objective is to force the solar subsystem to track the operating trajectory, which is the desired power generation, $P_{\text{s}}^{\text{ref}}$. We follow the controller design proposed in Ref. [23] to design this local controller. For the local controller associated with the RO water desalination, the objective is to regulate the retentate valve resistance to track the reference retentate flow velocity, $v_{\text{r}}^{\text{ref}}$. We adopt the method proposed in Ref. [35] to design a nonlinear model-based controller for the RO subsystem.

We note that the local controllers for wind/solar subsystems are designed based on sliding-mode control techniques and are robust with respect to uncertainty and yield essentially offset-free behavior [12,23].

4. Short-term supervisory predictive control of the integrated system

In this section, we focus on the stand-alone operating mode of the integrated system ($I_{\text{s}} = 0$) and design a supervisory con-

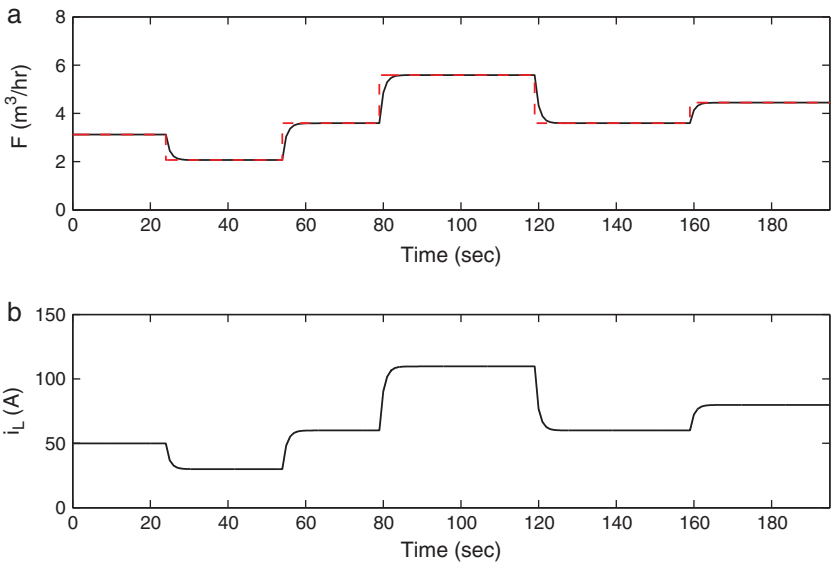

Fig. 7. Time-varying water demand F_d and corresponding load current i_L.

trol system to account for short-term optimal operation of the integrated system. We assume that the storage demand of the storage tank $F_s = 0$ to simplify the description of the controller formulation.

4.1. Supervisory control system design

Specifically, we re-design the supervisory MPC in Ref. [28] for the control of the integrated energy generation and water desalination system. In this proposed design, the supervisory MPC optimizes the power references P_w^{ref} and P_s^{ref} (operating points) of the wind and solar subsystems, respectively, but also takes into account the dynamics of the RO system. Note that in this design, i_b and v_r are not considered as decision variables in the formulation of the supervisory MPC because i_b is determined by the current balance of Eq. (12) in stand-alone operating mode and v_r^{ref} is determined by the water demand F_d. The primary control objective of the supervisory control system is to coordinate the wind and solar subsystems as well as the battery bank to provide enough energy to the RO system to satisfy the power demand of the scheduled water production. In addition, we try to reduce battery short-term charge–discharge cycles which can be caused by the variability of the renewable energy resources or the load demand. We operate the wind subsystem as the primary generation system and only activate the solar subsystem when the wind subsystem alone cannot satisfy the power demand. In the following, we first design

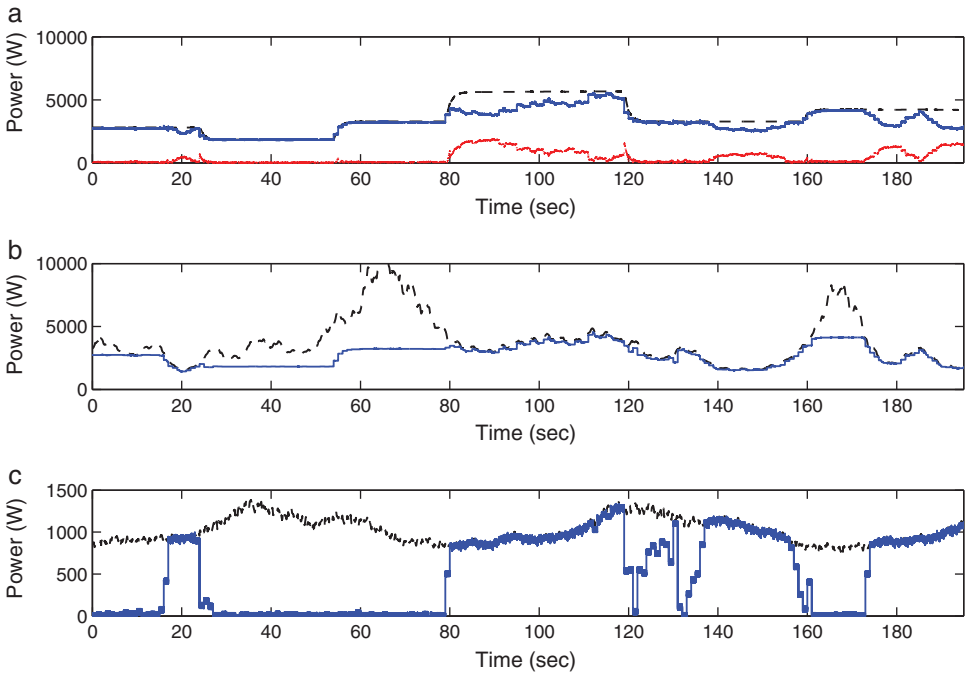

Fig. 8. (a) Generated power $P_w + P_s$ (solid line), total power demand P_T (dashed line) and power provided by battery bank P_b (dotted line); (b) Power generated by wind subsystem P_w (solid line) and maximum wind generation $P_{w,max}$ (dashed line); and (c) Power generated by solar subsystem P_s (solid line) and maximum solar generation $P_{s,max}$ (dashed line).

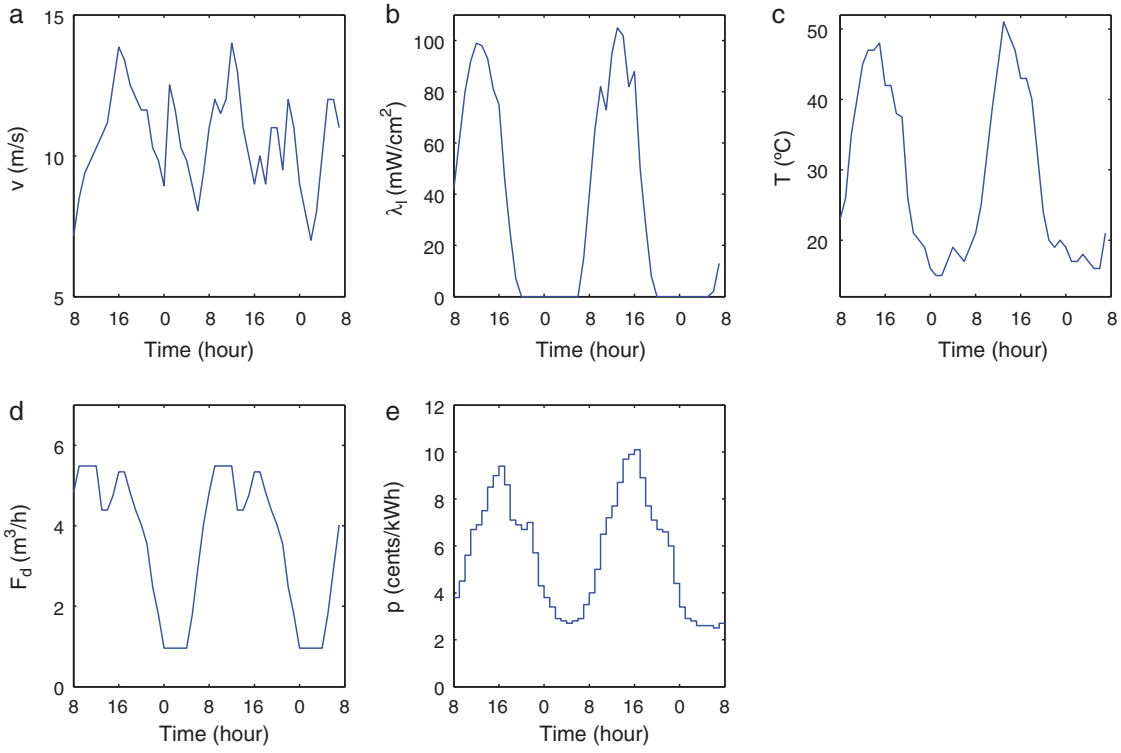

Fig. 9. Forecast of weather conditions, water demand and grid electricity price. (a) Wind speed v; (b) insolation λ_I; (c) PV panel temperature T; (d) water demand F_d, and (e) grid electricity price p.

the cost function used in the MPC to take into account the control objectives and then formulate the MPC based on the cost function. The supervisory control system is designed via MPC because it can take into account optimality considerations and handle state and input constraints. In this stand-alone operating mode, the operation strategy of the integrated energy generation system is as follows: (1) when the wind subsystem can generate enough energy to satisfy the total power demand, only the wind subsystem is activated and operated to track the power demand; (2) when the wind subsystem alone cannot generate enough energy to satisfy the total power demand, the solar subsystem is also activated to provide extra energy to satisfy the power demand; (3) when the two subsystems are not sufficient to complement the generation to satisfy the total power demand, the battery bank discharges to provide extra power to satisfy the load requirements. However, when the power limit that can be provided by the battery is surpassed, the load must be disconnected to recharge the battery and avoid damages.

We consider the case where the future water demand is known, that is $F_d(t)$ is known. We note that this assumption is a reasonable one given that there has been extensive work in short-term forecasting for weather conditions and municipal water demand [38]. The main implementation element of supervisory predictive control is that the supervisory controller is evaluated at discrete time instants $t_k = t_0 + k\Delta,\ k = 0, 1, \ldots,$ with t_0 being the initial time and Δ being the sampling time, and the optimal future power references, P_w^{ref} and P_s^{ref}, for a time period (prediction horizon) are obtained and only the first part (move) of the optimal reference trajectories are sent to the local control systems and implemented on the two units. In order to design this controller, first, a proper number of prediction steps, N, and a sampling time, Δ, are chosen. Before going to the formulation of the supervisory MPC, we design the cost function used in the MPC to take into account the control objectives. Specifically, the proposed design of the cost function is as follows:

$$J_s(t_k) = \int_{t_k}^{t_{k+N}} \alpha(P_{RO}(\tau) - P_w^{ref}(\tau) - P_s^{ref}(\tau))^2 d\tau + \int_{t_k}^{t_{k+N}} \beta P_s^{ref}(\tau)^2 d\tau + \int_{t_k}^{t_{k+N-1}} \zeta(P_b(\tau + \Delta) - P_b(\tau))^2 d\tau \quad (21)$$

where α, β and ζ are positive weighting factors on different terms. The first term in the cost function penalizes the difference between the power generated by the wind-solar system and the total power demand, which drives the wind and solar subsystems to satisfy the total demand to the maximum extent. Because there are infinite combinations of P_w^{ref} and P_s^{ref} that can minimize the first term, in order to allow only one solution to the optimization problem and to operate the wind subsystem as the primary generation system, we also put a small penalty on the reference power of the solar subsystem, P_s^{ref}. This term guarantees that the solar generation subsystem is only activated when the wind subsystem alone cannot satisfy the power demand. The third term in the cost function penalizes the change of the power provided by the battery bank to the load to reduce battery short-term charge–discharge cycles. Note that, if one wants to operate the solar system as the primary generation subsystem, the second term in the cost function can be modified to penalize the power reference of the wind subsystem. Note also that, other considerations (for example, charge of the battery bank) can be also taken into account in the design of the cost function by adding additional terms or modifying existing terms.

The proposed MPC design for the supervisory control system is as follows:

$$\min_{P_w^{ref}, P_s^{ref} \in S(\Delta)} J_s(t_k) \quad (22a)$$

$$\text{s.t.} \quad P_w^{ref}(\tau) \le \min_{\tau}\{P_w^{max}(\tau)\}, \quad \tau \in [t_{k+j}, t_{k+j+1}) \quad (22b)$$

$$P_s^{ref}(\tau) \le \min_{\tau}\{P_{PV,max}(\tau)\}, \quad \tau \in [t_{k+j}, t_{k+j+1}) \tag{22c}$$

$$P_w^{ref}(t_{k+j+1}) - P_w^{ref}(t_{k+j}) \le dP_{w,max} \tag{22d}$$

$$P_s^{ref}(t_{k+j+1}) - P_s^{ref}(t_{k+j}) \le dP_{s,max} \tag{22e}$$

$$\dot{\tilde{x}}(\tau) = f(\tilde{x}(\tau)) + g(\tilde{x}(\tau))u(\tau) \tag{22f}$$

$$h(\tilde{x}) = 0 \tag{22g}$$

$$\tilde{x}(0) = x(t_k) \tag{22h}$$

where $j = 0, \ldots, N-1$, $J_s(t_k)$ is the cost function to be minimized at time t_k, $P_w^{max}(\tau)$ and $P_s^{max}(\tau)$ are the maximum powers that can be generated by the wind and solar subsystems at time τ, respectively, $dP_{w,max}$ and $dP_{s,max}$ are the maximum allowable increasing values of P_w^{ref} and P_s^{ref} in two consecutive power references, $\tilde{x}$ is the predicted future state trajectory of the integrated system and $x(t_k)$ is the state measurement obtained at time t_k. We denote the optimal solution to the optimization problem of Eq. (22) as $P_{w,s}^{ref,*}(\tau|t_k)$ and $P_{s,s}^{ref,*}(\tau|t_k)$.

The power references of the wind and solar subsystems generated by the supervisory predictive controller of Eq. (22) are defined as follows:

$$\begin{aligned} P_w^{ref}(t) &= P_{w,s}^{ref,*}(t|t_k), \quad \forall \ t \in [t_k, t_{k+1}) \\ P_s^{ref}(t) &= P_{s,s}^{ref,*}(t|t_k), \quad \forall \ t \in [t_k, t_{k+1}) \end{aligned} \tag{23}$$

In the optimization problem of Eq. (22), the constraints of Eqs. (22b) and (22c) require that the computed power references should be smaller than the minimum of the maximum available within each sampling interval, which means the power references should be achievable for the wind and solar subsystems. The constraints of Eqs. (22d) and (22e) impose limits on the rate of change of the two power references. Note that the future maximum available powers for the wind and the solar subsystems are estimated using the information of future weather conditions forecast [12,23]. The constraints of Eqs. (22f) and (22g) are the system model of Eq. (20) with initial condition defined by Eq. (22h). The constraints of Eqs. (22b)–(22h) are inspired by results on the design of Lyapunov-based model predictive control systems (please see Refs. [39,40]).

4.2. Simulation results

In this subsection, we carry out simulations to demonstrate the effectiveness and applicability of the proposed supervisory MPC of Eq. (22). The sampling time and the prediction horizon of the MPC are chosen to be $\Delta = 1$ s and $N = 2$. Note that the choice of the prediction horizon is based on the fast dynamics of the wind-solar energy generation system and the RO system, the uncertainty associated with wind speed and is also made to achieve a balance between the evaluation time of the optimization problem of the supervisory MPC of Eq. (22) and of the desired closed-loop performance. The maximum increasing values of the two power references are chosen to be $dP_{w,max} = 1000$ W and $dP_{s,max} = 500$ W, respectively. The RO water desalination system is operated at a recovery rate $Y = 0.8$ and the overall power efficiency is assumed to be $\eta = 0.7$. The weighting factors in the cost function are chosen to be $\alpha = 1$, $\beta = 0.01$ and $\zeta = 0.4$.

We first carry out simulations under varying environmental conditions without disturbances. The time evolution of wind speed, PV panel temperature and insolation are shown in Fig. 3(a–c).

We consider time-varying water demand $F_d(t)$ with step changes as shown in Fig. 4(a) (dashed line). This water demand is reflected as a load current i_L with transient processes on the side of the energy generation system as shown in Fig. 4(b), which are due to the dynamic properties of the RO system.

The simulation results are shown in Fig. 5. It can be seen from Fig. 5(a) that the wind/solar/battery powers coordinate their behavior to meet the power demand of the RO system. Time evolution of output power and maximum available power from the wind subsystem and the solar subsystem are plotted in Fig. 5(b and c). When sufficient energy supply can be extracted from the two subsystems such as during 0–17 s, 25–78 s, 125–137 and 155–173 s, the battery is being recharged. In other periods, load demand is relatively high and the weather condition, which determines the maximum available generation capacity of the two subsystems, cannot permit sufficient energy supply. Thus, the supervisory controller drives the wind/solar subsystems to their instant maximum capacity and calls the battery bank for shortage compensation. Note that because of the dynamics of the RO desalination system, when there is a step change in the water demand, the RO desalination system takes a short time to track the water demand (see Fig. 4(a) (solid line)).

We have also carried out simulations to evaluate the robustness of the proposed supervisory control system of Eq. (22) subject to disturbances in wind speed and insolation; specifically, 10% variation in the wind speed and 5% variation in the insolation and additional high frequency disturbances to simulate real forecasting inaccuracy. The profiles of the wind speed and insolation are shown in Figs. 6(a and b). The simulation results are shown in Figs. 7 and 8. From these figures, we can see that the proposed supervisory control system of Eq. (22) operates in a robust fashion to coordinate the wind and solar subsystems as well as the battery bank to meet the total power demand of the desired water production.

We note that the simulations in this section were carried out in a computer with a Core 2 Duo 1.6 GHz processor. The MPC optimization problems were solved by Matlab built-in optimization solver *fmincon* and the average evaluation time was a little more than one minute. We also note that this evaluation time can be significantly reduced by code optimization, improved processor speed and model reduction.

5. Integration with the electrical grid and long-term operation

In this section, we focus on the electrical grid-connected operating mode of the integrated system ($I_s = 1$) and design a supervisory predictive control system to accomplish long-term optimal operation of the integrated system. The primary control objective is to regulate the integrated system to produce enough desalinated water to satisfy the total water consumption, F_d, and storage demand, F_s. The secondary objective is to take into account optimality considerations on system operation, for example, battery maintenance and time-varying electric power pricing. The supervisory control system determines the reference retentate flow rate (v_r^{ref}) for the RO water desalination subsystem and the current sent to the electrical grid (i_G^{ref}). In this case, the wind and solar subsystems operate at their maximum power generation points.

5.1. Supervisory control system design

In this supervisory MPC design, we explicitly take into account the following battery bank maintenance considerations [41,42]: (1) small charge/discharge currents are favorable; (2) the charge current should be constrained under a certain upper bound (we set the upper bound of the charge currents based on a simple taper charging approach [41]); (3) The depth of discharge (DOD) of the battery bank should not exceed d_b^{max} in order to protect the battery bank, and (4) the battery should be charged if extra generated power is available (in addition to satisfying water production power demand).

We also take into account the time-varying electric power pricing and try to achieve economically optimal operation by sending (selling) energy to the electrical grid at high electric power price and obtaining (buying) energy from the electrical grid at low electric power price. In order to send more energy to (or obtain less energy from) the electrical grid, we operate the RO water desalination subsystem at the energy optimal water recovery Y_{opt} so that the energy consumption per unit water produced is minimized [36].

In addition, we assume that there is a preferred SOS, s_t^{opt}, of the storage tank which is a balance between the capacities of the tank to supply unexpected water consumption demand and to store extra water production. We consider the case where the future water consumption demand of the RO subsystem is known; that is, $F_d(t)$, is known. We also assume that future hourly weather conditions (i.e., wind speed, insolation, photovoltaic cell temperature) forecast information is available.

The cost function of the proposed supervisory controller is designed as follows:

$$J_g(t_k) = \gamma \int_{t_k}^{t_{k+N}} d_b(\tau)d\tau + \xi \int_{t_k}^{t_{k+N}} i_b(\tau)^2 d\tau + \zeta \int_{t_k}^{t_{k+N}} p(\tau)P_G(\tau)d\tau + \varepsilon \int_{t_k}^{t_{k+N}} \left| s_t(\tau) - s_t^{opt} \right| d\tau + \theta \frac{\int_{t_k}^{t_{k+N}} P_{RO}(\tau)d\tau}{\int_{t_k}^{t_{k+N}} F_p(\tau)d\tau} \quad (24)$$

where γ, ξ, ζ, ε, and θ are positive weighting factors, $p(\tau)$ denotes the time-varying electric power price and P_G ($P_G = -i_G v_b$) is the power drawn from the electrical grid by the integrated system. In this cost function, the first term implies that the battery should be charged if the battery is not fully charged; the second term takes into account that small charge currents are preferred; the third term is used to account for the economic optimization consideration by selling/buying power to/from the electrical grid; the fourth term is used to make sure that the water level in the storage tank is maintained around the optimal water level; and the fifth term penalizes the power consumption per unit of permeate water produced.

For this case, the proposed MPC design for the supervisory control system at time t_k is as follows:

$$\min_{i_G^{ref}, v_r^{ref} \in S(\Delta)} J_g(t_k) \quad (25a)$$

$$\text{s.t.} \quad P_{RO}(\tau) - P_w(\tau) - P_s(\tau) + i_G^{ref}(\tau)v_b(\tau) + i_b v_b = 0 \quad (25b)$$

$$F_p^{min} \le F_p(\tau) \le F_p^{max} \quad (25c)$$

$$0 \le d_b(\tau) \le d_b^{max} \quad (25d)$$

$$s_t^{min} \le s_t(\tau) \le s_t^{max} \quad (25e)$$

$$i_b(\tau) \le i_b^{max}(s_b(\tau)) \quad (25f)$$

$$\dot{\tilde{x}}(\tau) = f(\tilde{x}(\tau)) + g(\tilde{x}(\tau))u(\tau) \quad (25g)$$

$$h(\tilde{x}) = 0 \quad (25h)$$

$$\tilde{x}(0) = x(t_k) \quad (25i)$$

We denote the optimal solution to the optimization problem of Eq. (25) as $i_G^{ref,*}(\tau|t_k)$ and $v_r^{ref,*}(\tau|t_k)$. The references of battery charge/discharge current and of the RO retentate flow rate sent to the local controllers by the supervisory controller of Eq. (22) are defined as follows:

$$\begin{aligned} i_G^{ref}(t) &= i_G^{ref,*}(t|t_k), \quad \forall \ t \in [t_k, t_{k+1}), \\ v_r^{ref}(t) &= v_r^{ref,*}(t|t_k), \quad \forall \ t \in [t_k, t_{k+1}). \end{aligned} \quad (26)$$

In the optimization problem of Eq. (25), the constraint of Eq. (25b) is an energy balance for the integrated system. The constraint of Eq. (25c) imposes upper and lower bounds (F_p^{max} and F_p^{min}, respectively) on the permeate flow rate F_p, which are used to guarantee the equipment safety of the membrane module in the RO water desalination subsystem. The constraint of Eq. (25d) requires that the depth of discharge of the battery bank should not exceed d_b^{max}. The constraint of Eq. (25e) imposes upper and lower bounds on the water level in the storage tank. The constraint of Eq. (25f) places an upper bound on the charge current of the battery bank and this upper bound is a function of the current depth of discharge of the battery bank. The constraints of Eqs. (25g) and (25h) are the system model of Eq. (20) with initial condition defined by Eq. (25i).

Note that the dynamics of the integrated system exhibit a two-time-scale behavior. Specifically, the dynamics of the states, i_q, i_d, w_e, w_{PV}, i_s and v_r, are relatively fast (in the order of seconds); and the dynamics of the states, v_c and h_l, are relatively slow (in the order of minutes). In order to achieve long-term system optimal operation, we take advantage of this two-time-scale property in the design of the supervisory MPC design of Eq. (25) to significantly reduce the evaluation time of the MPC. Specifically, in the evaluation of the MPC of Eq. (25), only the slow system dynamics is taken into account and the fast system states that are (explicitly or implicitly) used in the MPC are estimated by the computed future operating trajectories (decision variables of the MPC). For example, in the calculation of future $F_p(\tau)$, the fast state v_r is assumed to be equal to v_r^{ref}.

5.2. Simulation results

We carry out a closed-loop simulation to demonstrate the applicability and effectiveness of the supervisory MPC of Eq. (25) in achieving efficient integration of the wind/solar/RO system with the electrical grid. The prediction horizon and the sampling time of the MPC are chosen to be $N = 24$ and $\Delta = 1$ h taking into account that the water demand (for example, of a community) usually presents periodic fluctuations with a period of 24 h. The weighting factors in the cost function are chosen to be $\gamma = 0.001$, $\xi = 1.8 \times 10^{-7}$, $\zeta = 1 \times 10^{-6}$, $\varepsilon = 0.01$ and $\theta = 2 \times 10^{-7}$. The overall RO system pump power efficiency is assumed to be $\eta = 0.7$, the upper bound on d_b is $d_b^{max} = 0.8$, the lower and upper bounds on F_p are $F_p^{min} = 0.1814\,m^3/h$ and $F_p^{max} = 3.9918\,m^3/h$, respectively, and the lower and upper bounds on s_t are $s_t^{min} = 0$ and $s_t^{max} = 1$, respectively.

Specifically, we carry out simulations for one day (24 h) starting at 8 a.m. We assume that hourly weather forecast, hourly water demand and hourly grid electricity price are available to the supervisory MPC for the entire 24-h period. A two-day forecast information of weather conditions, water demand and grid electricity price, used in our simulations, is shown in Fig. 9. We also introduce up to 15%, 10% and 10% deviations and additional high frequency disturbances to simulate the forecasting inaccuracy for wind-speed, PV cell temperature and isolation, respectively, and also introduce a low frequency disturbance in the water demand. The actual weather conditions and water demand along with real-time electricity price variations are shown in Fig. 10. Fig. 11 displays the time evolutions of power generation by the wind and solar subsystems and power consumption by the RO subsystem. Fig. 10(a and b) shows that in this scenario the supervisory MPC forces the wind/solar subsystems to track the maximum power generation points all the time. Fig. 12(a) shows the profile of power trading of the system with the grid. We denote the power purchased from the grid as positive and the power sold to the grid as negative. It can be seen that the supervisory MPC controller outputs optimal grid power trading references at each sampling time taking into account one day ahead variations of electricity price, states of battery bank and water tank as well as wind/solar power generation capabilities.

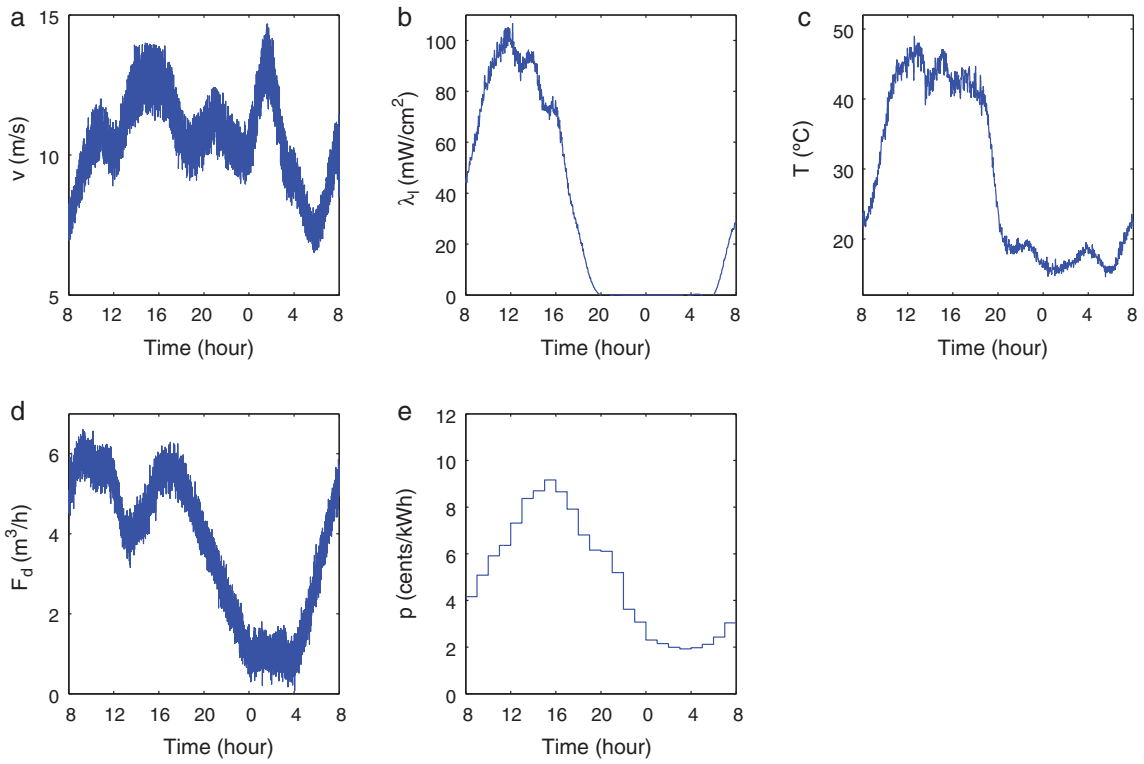

Fig. 10. Weather conditions, water demand and grid electricity price including realistic variations. (a) Wind speed v; (b) insolation λ_I; (c) PV panel temperature T; (d) water demand F_d, and (e) grid electricity price p.

Note that the periods when grid power is fluctuating indicates that part of battery current is diverted to the grid at that moment so that the upper battery current limit cannot be exceeded. Consequently, profiting from power trading is achieved while system performance is optimized. The cumulative revenue of power trading is shown in Fig. 12(b).

In addition to efficient grid integration, an advantage of our supervisory MPC design is that it is able to schedule water production to be smooth (nearly uniform with respect to time) by taking into account future conditions/demand variations and by coordinating the subsystems. Given a total amount of water demand, uniformly producing water is not only beneficial in terms of equip-

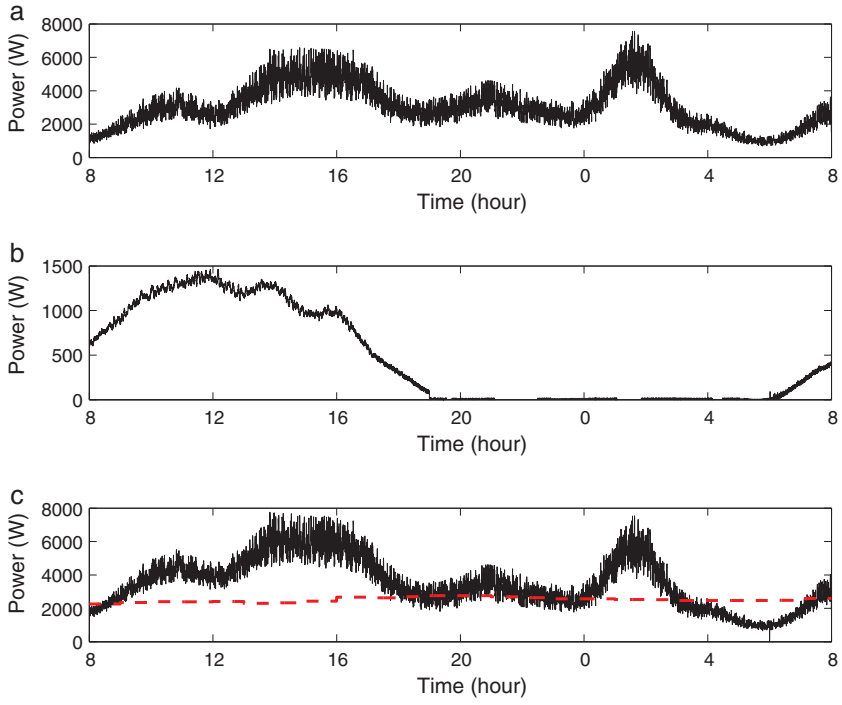

Fig. 11. Power generation and consumption. (a) Power generated by the wind subsystem P_w; (b) Power generated by the solar subsystem P_s; (c) Generated power $P_w + P_s$ (solid line) and total power demand P_{RO} (dashed line).

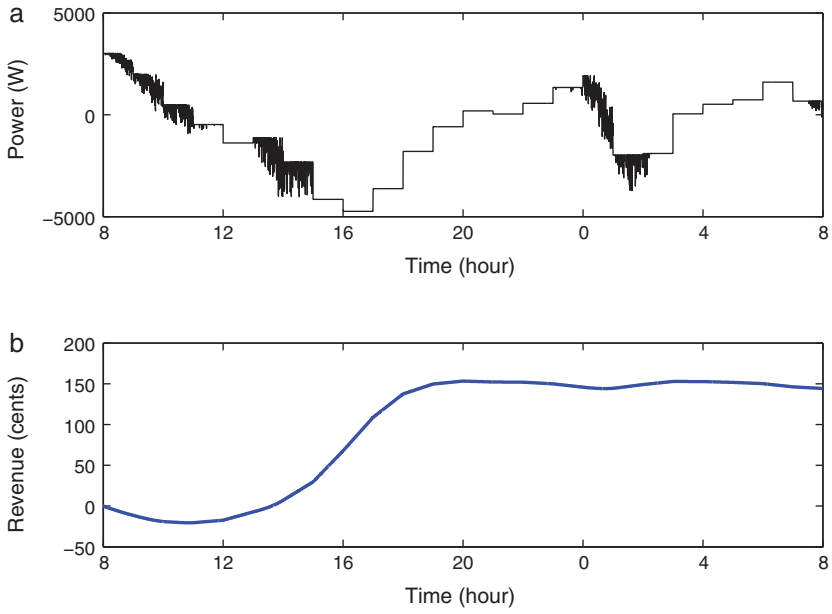

Fig. 12. (a) Electrical grid power trading profile P_G and (b) Cumulative revenue of power trading with the grid.

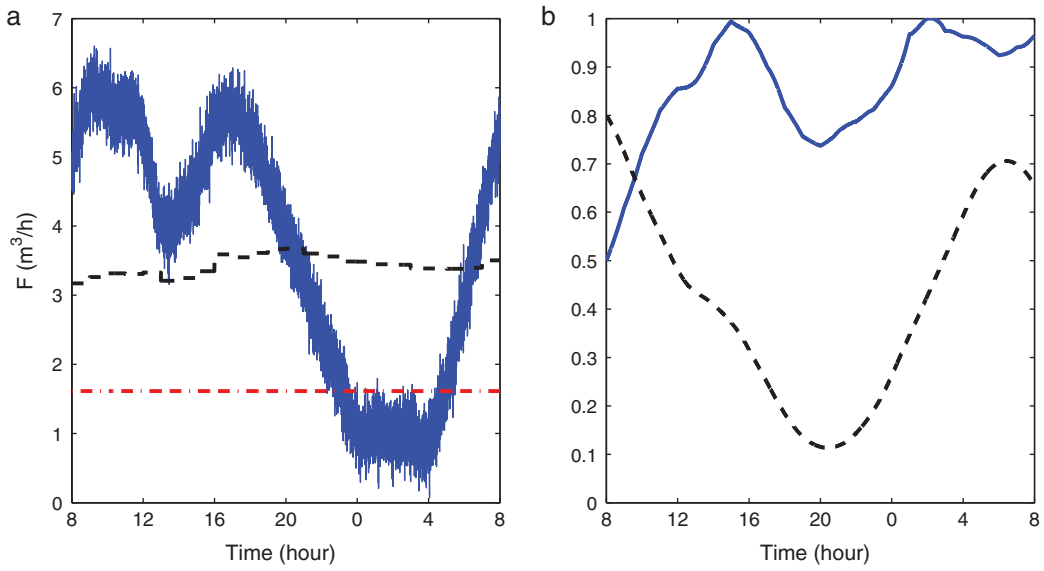

Fig. 13. (a) Rate of water demand F_d (solid line), permeate flow rate F_p (dashed line) and the energy-efficient production flow rate F_s (dash-dotted line); (b) Battery state of charge s_b (solid line) and water tank state of storage s_t (dashed line).

ment maintenance, but it also consumes a smaller amount of energy as well. In fact, deviation from the optimal operating point as specified in Fig. 13(a) results in additional energy consumption. It can be seen from Fig. 13(a) that water production is relatively smooth despite significantly varying water demand and weather conditions during a day. This is largely due to the optimized utilization of capacities of the battery bank and of the water tank as well as integration with the electrical grid, which jointly act as buffers against external fluctuations. The states of charge of the battery bank and of storage of the water tank are shown in Fig. 13(b), displaying, as expected, periodic variations.

We note that the simulations in this section were carried out in a computer with a Core 2 Quad 2.66 GHz processor. The MPC optimization problems were solved using the open source interior point optimizer Ipopt and the average evaluation time was less than 0.5 s, which is sufficiently fast compared with the sampling interval of 1 h. We note that the reduction in the evaluation time compared to the one in Section 4.2 is primarily due to the use of a reduced-order process model in the optimization problem.

6. Conclusions

In order to enable the development of the "smart electrical grid", we proposed a conceptual distributed control framework for electrical grid integrated with distributed renewable energy generation systems. We first introduced the different elements and their interactions in the distributed control framework. Then, we focused on a specific wind/solar energy generation system connected to a RO water desalination system and the electrical grid and designed a supervisory predictive controller via MPC to operate the integrated system taking into account short-term optimal maintenance and operation considerations. Subsequently, we designed a supervisory MPC for long-term optimal operation of the integrated

system accounting for battery maintenance and time-varying electric power pricing. Simulations were carried out to illustrate the applicability and effectiveness of the proposed designs.

References

[1] S. Massoud Amin, B.F. Wollenberg, Toward a smart grid, IEEE Power & Energy Magazine 3 (2005) 34–41.
[2] U.S. Department of Energy, The smart grid: an introduction, Technical Report, 2008.
[3] National Institute of Standards and Technology, NISF framework and roadmap for smart grid interoperability standards, 2010.
[4] California Energy Commission, Integrating new and emerging technologies into the California smart grid infrastructure, Technical Report, 2008.
[5] R. Spee, J.H. Enslin, Novel control strategies for variable-speed doubly fed wind power generation systems, Renewable Energy 6 (1995) 907–915.
[6] P. Novak, T. Ekelund, Y. Jovik, B. Schmidtbauer, Modeling and control of variable-speed wind-turbine drive system dynamics, IEEE Control Systems Magazine 15 (1995) 28–37.
[7] T. Thiringer, J. Linders, Control by variable rotor speed of fixed-pitch wind turbine operating in speed range, IEEE Transactions on Energy Conversion 8 (1993) 520–526.
[8] M.G. Simoes, B.K. Bose, R.J. Spiegel, Fuzzy logic based intelligent control of a variable speed cage machine wind generation system, IEEE Transactions on Power Electronics 12 (1997) 87–95.
[9] K. Uhlen, B.A. Foss, O.B. Gjosaeter, Robust control and analysis of a wind-diesel hybrid power plant, IEEE Transactions on Energy Conversion 9 (1994) 701–708.
[10] F. Valenciaga, P.F. Puleston, R.J. Mantz, P.E. Battaiotto, An adaptive feedback linearization strategy for variable speed wind energy conversion systems, International Journal of Energy Research 24 (2000) 151–161.
[11] K. Tan, S. Islam, Optimum control strategies in energy conversion of PMSG wind turbine system without mechanical sensors, IEEE Transactions on Energy Conversion 19 (2004) 392–399.
[12] F. Valenciaga, P.F. Puleston, P.E. Battaiotto, Variable structure system control design method based on a differential geometric approach: application to a wind energy conversion subsystem, IEE Proceedings: Control Theory and Applications 151 (2004) 6–12.
[13] M. Chinchilla, S. Arnaltes, J.C. Burgos, Control of permanent-magnet generators applied to variable-speed wind-energy systems connected to the grid, IEEE Transactions on Energy Conversion 21 (2006) 130–135.
[14] F. Valenciaga, P.F. Puleston, High-order sliding control for a wind energy conversion system based on a permanent magnet synchronous generator, IEEE Transactions on Energy Conversion 23 (2008) 860–867.
[15] D.Q. Dang, Y. Wang, W. Cai, Nonlinear model predictive control (NMPC) of fixed pitch variable speed wind turbine, in: Proceedings of 2008 IEEE International Conference on Sustainable Energy Technologies, Singapore, Singapore, 2008, pp. 29–33.
[16] M.S. Khan, M.R. Iravani, Hybrid control of a grid-interactive wind energy conversion system, IEEE Transactions on Energy Conversion 23 (2008) 895–902.
[17] T.A. Johansen, C. Storaa, Energy-based control of a distributed solar collector field, Automatica 38 (2002) 1191–1199.
[18] F. Coito, J.M. Lemos, R.N. Silva, E. Mosca, Adaptive control of a solar energy plant: exploiting accessible disturbances, International Journal of Adaptive Control and Signal Processing 11 (1997) 327–342.
[19] E.F. Camacho, M. Berenguel, Robust adaptive model predictive control of a solar plant with bounded uncertainties, International Journal of Adaptive Control and Signal Processing 11 (1997) 311–325.
[20] N. Hamrouni, M. Jraidi, A. Cherif, New control strategy for 2-stage grid-connected photovoltaic power system, Renewable Energy 33 (2008) 2212–2221.
[21] T. Yoshida, K. Ohniwa, O. Miyashita, Simple control of photovoltaic generator systems with high-speed maximum power point tracking operation, EPE Journal 17 (2007) 38–42.
[22] F. Valenciaga, P.F. Puleston, P.E. Battaiotto, R.J. Mantz, Passivity/sliding mode control of a stand-alone hybrid generation system, IEE Proceedings: Control Theory and Applications 147 (2000) 680–686.
[23] F. Valenciaga, P.F. Puleston, P.E. Battaiotto, Power control of a photovoltaic array in a hybrid electric generation system using sliding mode techniques, IEE Proceedings: Control Theory and Applications 148 (2001) 448–455.
[24] F. Valenciaga, P.F. Puleston, Supervisor control for a stand-alone hybrid generation system using wind and photovoltaic energy, IEEE Transactions on Energy Conversion 20 (2005) 398–405.
[25] N.A. Ahmed, M. Miyatake, A.K. Al-Othman, Hybrid solar photovoltaic/wind turbine energy generation system with voltage-based maximum power point tracking, Electric Power Components and Systems 37 (2009) 43–60.
[26] Y. Chen, J. Wu, Agent-based energy management and control of a grid-connected wind/solar hybrid power system, in: C.L. Gu, K. Yang, J. Wang (Eds.), Proceedings of the 2008 11th International Conference on Electrical Machines and Systems, Wuhan, China, 2008, pp. 2362–2365.
[27] M. Dali, J. Belhadj, X. Roboam, Hybrid solar-wind system with battery storage operating in grid-connected and standalone mode: control and energy management—experimental investigation, Energy 35 (2010) 2587–2595.
[28] W. Qi, J. Liu, X. Chen, P.D. Christofides, Supervisory predictive control of standalone wind-solar energy generation systems, IEEE Transactions on Control Systems Technology 19 (2011) 199–207.
[29] W. Qi, J. Liu, P.D. Christofides, Supervisory predictive control for long-term scheduling of an integrated wind/solar energy generation and water desalination system, IEEE Transactions on Control Systems Technology (2011), doi:10.1109/TCST.2011.2119318.
[30] J.B. Rawlings, B.T. Stewart, Coordinating multiple optimization-based controllers: new opportunities and challenges, Journal of Process Control 18 (2008) 839–845.
[31] J. Liu, D. Muñoz de la Peña, P.D. Christofides, Distributed model predictive control of nonlinear process systems, AIChE Journal 55 (2009) 1171–1184.
[32] J. Liu, X. Chen, D. Muñoz de la Peña, P.D. Christofides, Sequential and iterative architectures for distributed model predictive control of nonlinear process systems, AIChE Journal 56 (2010) 2137–2149.
[33] P.D. Christofides, J. Liu, D. Muñoz de la Peña, Networked and Distributed Predictive Control: Methods and Applications to Nonlinear Process Networks, Advances in Industrial Control Series, Springer-Verlag, London, 2011.
[34] A.N. Venkat, I.A. Hiskens, J.B. Rawlings, S.J. Wright, Distributed MPC strategies with application to power system automatic generation control, IEEE Transactions on Control Systems Technology 16 (2008) 1192–1206.
[35] A.R. Bartman, P.D. Christofides, Y. Cohen, Nonlinear model-based control of an experimental reverse-osmosis water desalination system, Industrial & Engineering Chemistry Research 48 (2009) 6126–6136.
[36] A. Zhu, A. Rahardianto, P.D. Christofides, Y. Cohen, Reverse osmosis desalination with high permeability membranes—cost optimization and research needs, Desalination and Water Treatment 15 (2010) 256–266.
[37] A. Zhu, P.D. Christofides, Y. Cohen, Effect of thermodynamic restriction on energy cost optimization of RO membrane water desalination, Industrial & Engineering Chemistry Research 48 (2009) 6010–6021.
[38] M. Ghiassi, D.K. Zimbra, H. Saidane, Urban water demand forecasting with a dynamic artificial neural network model, Journal of Water Resources Planning and Management 134 (2008) 138–146.
[39] P.D. Christofides, N.H. El-Farra, Control of Nonlinear and Hybrid Process Systems: Designs for Uncertainty Constraints and Time-Delays, Springer-Verlag, Berlin, Germany, 2005.
[40] P. Mhaskar, N.H. El-Farra, P.D. Christofides, Stabilization of nonlinear systems with state and control constraints using Lyapunov-based predictive control, Systems and Control Letters 55 (2006) 650–659.
[41] D. Linden, T.B. Reddy (Eds.), Handbook of Batteries, 3rd ed., McGraw-Hill, 2002.
[42] A.J. Ruddell, A.G. Dutton, H. Wenzl, C. Ropeter, D.U. Sauer, J. Merten, C. Orfanogiannis, J.W. Twidell, P. Vezin, Analysis of battery current microcycles in autonomous renewable energy systems, Journal of Power Sources 112 (2002) 531–546.